Anomalies in B-meson decays and the muon $g-2$ from dark loops

Da Huang,[1,2,*] António P. Morais,[1,†] and Rui Santos[3,4,‡]

[1]Departamento de Física da Universidade de Aveiro and CIDMA, Campus de Santiago, 3810-183 Aveiro, Portugal
[2]National Astronomical Observatories, Chinese Academy of Sciences, Beijing, 100012, China
[3]Centro de Física Teórica e Computacional, Faculdade de Ciências, Universidade de Lisboa, Campo Grande, Edifício C8 1749-016 Lisboa, Portugal
[4]ISEL—Instituto Superior de Engenharia de Lisboa, Instituto Politécnico de Lisboa 1959-007 Lisboa, Portugal

(Received 11 August 2020; accepted 17 September 2020; published 9 October 2020)

We explore a class of models which can provide a common origin for the recently observed evidence for lepton flavor universality violation in $b \to s l^+ l^-$ decays, the dark matter (DM) problem, and the long-standing muon $(g-2)$ anomaly. In particular, both anomalies in the B meson decays and the muon $(g-2)$ can be explained by the additional one-loop diagrams with DM candidates. We first classify several simple models according to the new fields' quantum numbers. We then focus on a specific promising model and perform a detailed study of both DM and flavor physics. A random scan over the relevant parameter space reveals that there is indeed a large parameter space which can explain the three new physics phenomena simultaneously, while satisfying all other flavor and DM constraints. Finally, we discuss some of the possible new physics signatures at the Large Hadron Collider.

DOI: 10.1103/PhysRevD.102.075009

I. INTRODUCTION

One of the most recent hints of new physics (NP) comes from the observed anomalies in the semileptonic decay rates of the B meson, which suggests a violation of lepton flavor universality. Concretely, the most precise measurement of the ratios of the exclusive branching fractions, $R(K^{(*)}) = \mathcal{B}(B \to K^{(*)}\mu^+\mu^-)/\mathcal{B}(B \to K^{(*)}e^+e^-)$, is the one by the LHCb Collaboration [1,2], with the following values

$$R(K) = 0.846^{+0.060+0.016}_{-0.054-0.014}, \qquad q^2 \in [1.1, 6]\ \mathrm{GeV}^2, \tag{1}$$

and

$$R(K^*) = \begin{cases} 0.660^{+0.110}_{-0.070} \pm 0.024, & q^2 \in [0.045, 1.1]\ \mathrm{GeV}^2, \\ 0.685^{+0.113}_{-0.069} \pm 0.047, & q^2 \in [1.1, 6]\ \mathrm{GeV}^2. \end{cases} \tag{2}$$

where q^2 is the dilepton mass squared in the processes, while the corresponding Standard Model (SM) predictions are [3,4]

$$R(K) = 1.0004(8), \qquad q^2 \in [1.1, 6]\ \mathrm{GeV}^2, \tag{3}$$

and

$$R(K^*) = \begin{cases} 0.920 \pm 0.007, & q^2 \in [0.045, 1.1]\ \mathrm{GeV}^2, \\ 0.996 \pm 0.002, & q^2 \in [1.1, 6]\ \mathrm{GeV}^2. \end{cases} \tag{4}$$

More recently, the Belle Collaboration has published their measurements on these two important quantities in Refs. [5,6], with larger error bars compared with the LHCb results. One should note that the quantities $R(K^{(*)})$ are very clean probes of NP because the theoretical and experimental uncertainties related to the hadronic matrix elements cancel out [3]. Further evidence supporting this B physics anomaly has been obtained by measuring other observables in rare B meson decays, such as the differential branching ratios [7–9] and angular distribution observables [10–17] in the processes $B \to \phi\mu^+\mu^-$ and $B \to K^{(*)}\mu^+\mu^-$, which have also shown deviations from their SM predictions. Note that all anomalies are associated with the transition $b \to s\mu^+\mu^-$. In order to reconcile these discrepancies, many models have been proposed. One such type of models have lepton universality violation at tree level by introducing a Z' [18–22] or a leptoquark [23–29], see e.g., Refs. [30–32] for

*dahuang@ua.pt
†aapmorais@ua.pt
‡rasantos@fc.ul.pt

recent reviews and references therein. One can also interpret the experimental data by one-loop penguin and box diagrams involving new exotic particles [33–37]. More recently, it has been pointed out in Ref. [38] that the inclusion of the unknown EW or QED corrections may also affect the analysis of $R(K^{(*)})$.

Besides the above NP signals in B meson decays, there are other important hints like the long-standing low-energy flavor anomaly involving the measurement of the anomalous magnetic moment of the muon, $(g-2)_\mu$ [39,40]. The most recent prediction of this quantity in the SM [41] has shown a 3.7σ discrepancy from the experimental measurement [42]:

$$\Delta a_\mu = a_\mu^{\rm exp} - a_\mu^{\rm SM} \simeq (27.4 \pm 7.3) \times 10^{-10}, \qquad (5)$$

where the error is obtained by combining the theoretical and experimental uncertainties. In the near future, a great reduction in the experimental uncertainty is expected, with the results from the experiments at J-PARC [43] and Fermilab [44]. A further demand for NP arises from the increasing number of experiments pointing to the existence of dark matter (DM) in our Universe [39,45,46]. However, despite the great experimental and theoretical efforts in detecting DM particles [45] during the last decades, the nature of DM remains a mystery in particle physics. The DM problem has already been investigated in various models [47] which also address the B meson decay anomalies, such as, e.g., Refs. [48–62] for Z' models, Refs. [63–67] for leptoquark models, and Refs. [68–73] for models with one-loop solutions.

In the present paper, we propose to simultaneously solve all of the three above NP issues by constructing a class of models inspired by the model in Ref. [71], in which the DM was provided by a neutral $SU(2)_L$ singlet vectorlike fermion stabilized by a new Z_2 symmetry. By further introducing two extra scalar fields, one $SU(3)_c$ colored while the other colorless, the lepton universality violation observed in B meson decays was solved by the NP one-loop contributions. We will extend this model by considering several simple variations of the $SU(2)_L \times U(1)_Y$ charge assignment of the newly introduced particles. Concretely, we will focus on models in which the $SU(2)_L$ representations of these particles are either singlet, doublet, or triplet, and the vectorlike fermions have integer electric charge with values 0 or ± 1. We will list all models satisfying these conditions and will identify the possible DM candidate in each model. After that, we will study in detail the DM and flavor phenomenology in one of the most promising models in this class. In our discussion, we will perform a scan in the parameter space of physical interest and identify regions which can solve the muon $g-2$ anomaly and the B meson decay anomaly while providing a viable DM candidate.

The paper is organized as follows. In Sec. II, we extend the model in Ref. [71] by listing all possible simple charge variations. Whenever possible we identify the DM candidate in each model. In the following sections, we discuss one specific model in this list. In Sec. III, we write down the corresponding NP Lagrangian. The flavor observables are calculated analytically in Sec. IV, including the muon anomalous magnetic moment, $b \to s\mu^+\mu^-$, the mass difference in the B_s-$\bar{B}_s$ mixing, and $b \to s\gamma$. In Sec. V, we address the DM phenomenology as predicted by this model. Specifically, we consider the constraints from DM relic density, DM direct detections and the invisible Higgs decay. In Sec. VI we present the numerical results of our scan by taking all of the flavor and DM observables into account. Finally, conclusions and further discussions on collider signatures are given in Sec. VII.

II. A LIST OF POSSIBLE MODELS

As discussed above we want to generalize the model proposed in Ref. [71] by extending the dark sector particles to other $SU(2)_L \times U(1)_Y$ representations. The classification is based on the representation of the new fermion χ, belonging to the Z_2 odd sector, which either belongs to the singlet, doublet, or triplet $SU(2)_L$ representation and has a $U(1)_Y$ hypercharge such that the electric charge is either 0, where it can become a DM candidate, or ± 1. The charges of the remaining new fields can be determined from the existence of the following Yukawa interaction

$$\mathcal{L}_{\rm int}^{\rm NP} = y_{Q_i} \bar{Q}_{Li} \Phi_q \chi_R + y_{Li} \bar{L}_{Li} \Phi_l \chi_R + \text{H.c.}, \qquad (6)$$

where Φ_q and Φ_l are two spin zero fields, a triplet and a singlet of $SU(3)_c$ respectively; y_{Q_i} and y_{Li} are constants and Q_{Li} and L_{Li} are the usual SM left-handed doublets for quarks and leptons respectively. This Lagrangian is required to provide the one-loop solution to the B anomalies as shown in Fig. 1.

We impose a new Z_2 symmetry under which the new particles Φ_q, Φ_l and χ are all odd while all SM particles are even. With this charge assignment, the lightest color- and electromagnetically-neutral Z_2-odd particle can provide a DM candidate. Furthermore, we assume that χ is a vectorlike fermion with its left- and right-handed components

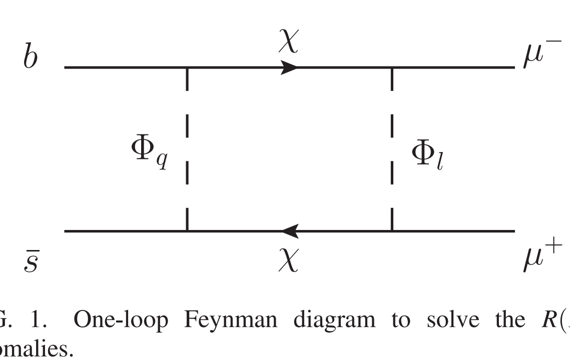

FIG. 1. One-loop Feynman diagram to solve the $R(K^{(*)})$ anomalies.

TABLE I. Charge assignment for the Z_2-odd fields in Model 1.

	$SU(3)_c$	$SU(2)_L$	$U(1)_Y$
χ_R	**1**	**1**	0
Φ_l	**1**	**2**	$-1/2$
Φ_q	**3**	**2**	$1/6$

written as χ_L and χ_R. However, note that only χ_R is involved in the interaction of Eq. (6). Note also that, if χ is in a self-conjugate representation of $SU(2)_L$ with zero $U(1)_Y$ charge, we only need to introduce the right-handed component χ_R since its Majorana mass term can arise in this case. This will be the case in two of the models presented. Otherwise χ_L has to be introduced.

In the remainder of this section, we list all possible NP models satisfying the restrictions above. Along with each model we identify the possible DM candidates.

(i) Model 1: The charge assignment for the Z_2-odd fields in this model is given in Table I, which is exactly the same as the one studied in Ref. [71]. However, we would like to make some comments regarding this charge assignment. Since χ_R and the neutral component in Φ_l are electric- and color-neutral, either particle can be the DM candidate. Note that χ_R is self-conjugate, so we can introduce a Majorana mass term for it. Thus, if χ_R is the DM particle in this model, we do not need to introduce its left-handed partner χ_L. Furthermore, together with the following term

$$(\Phi_l i\sigma_2 H)^2 + \text{H.c.}, \tag{7}$$

where H is the SM Higgs doublet, the Lagrangian breaks lepton number conservation by two units. Thus, the model can generate a nonzero Majorana neutrino mass at the one-loop level. In fact, this case is exactly the famous scotogenic model with the radiative neutrino mass generation proposed by Ernest Ma in Ref. [74].

(ii) Model 2: Table II lists the quantum numbers for the fields in this model. Since there is no electrically neutral particle in the spectrum, there is no DM candidate, and we will no longer consider it.

(iii) Model 3: The charge assignment for the fields is given in Table III, where the DM candidate can only be the neutral component contained in the doublet scalar Φ_l.

TABLE II. Charge assignment for the Z_2-odd fields in Model 2.

	$SU(3)_c$	$SU(2)_L$	$U(1)_Y$
χ_R	**1**	**1**	1
Φ_l	**1**	**2**	$-3/2$
Φ_q	**3**	**2**	$-5/6$

TABLE III. Charge assignment for the Z_2-odd fields in Model 3.

	$SU(3)_c$	$SU(2)_L$	$U(1)_Y$
χ_R	**1**	**1**	-1
Φ_l	**1**	**2**	$1/2$
Φ_q	**3**	**2**	$7/6$

TABLE IV. Charge assignment for the Z_2-odd fields in Model 4.

	$SU(3)_c$	$SU(2)_L$	$U(1)_Y$
χ_R	**1**	**2**	$1/2$
Φ_l	**1**	**1**	-1
Φ_q	**3**	**1**	$-1/3$

(iv) Model 4: Table IV shows the charge assignment for this model, where the DM particle can only be the neutral component contained in the fermionic doublet χ.

(v) Model 5: From the SM gauge group charges shown in Table V, we see that there are two DM candidates in this model: one is the singlet scalar Φ_l and the other is the neutral component of the vectorlike fermion doublet χ.

(vi) Model 6: We show the SM gauge group charges of new Z_2-odd particles in Table VI. Note that χ_R is self-conjugate, which guarantees the anomaly cancellation without the need of its left-handed component. Rather, we can introduce the Majorana mass term for χ_R: $m_\chi \bar{\chi}_R^c \chi_R + \text{H.c.}$. Thus, like in Model 1, small Majorana neutrino masses can be generated for active neutrinos [75].

(vii) Model 7: Table VII gives the charge assignment for this model, in which the only choice for DM is the neutral component in the triplet χ.

TABLE V. Charge assignment for the Z_2-odd fields in Model 5.

	$SU(3)_c$	$SU(2)_L$	$U(1)_Y$
χ_R	**1**	**2**	$-1/2$
Φ_l	**1**	**1**	0
Φ_q	**3**	**1**	$2/3$

TABLE VI. Charge assignment for the Z_2-odd fields in Model 6.

	$SU(3)_c$	$SU(2)_L$	$U(1)_Y$
χ_R	**1**	**3**	0
Φ_l	**1**	**2**	$-1/2$
Φ_q	**3**	**2**	$1/6$

TABLE VII. Charge assignment for the Z_2-odd fields in Model 7.

	$SU(3)_c$	$SU(2)_L$	$U(1)_Y$
χ_R	**1**	**3**	1
Φ_l	**1**	**2**	$-3/2$
Φ_q	**3**	**2**	$-5/6$

TABLE VIII. Charge assignment for the Z_2-odd fields in Model 8.

	$SU(3)_c$	$SU(2)_L$	$U(1)_Y$
χ_R	**1**	**3**	-1
Φ_l	**1**	**2**	$1/2$
Φ_q	**3**	**2**	$7/6$

(viii) Model 8: We show the color- and EW-charges of new particles in Table VIII. Here the DM can be the neutral component in either the scalar doublet Φ_l^0 or the fermionic triplet χ^0.

Finally, we would like to remark that if we swap the spins $0 \leftrightarrow 1/2$ for new particles in the above models, we can generate other 8 models. For instance, if we exchange the spins of particles in Table IV, the obtained model corresponds to the one studied in Ref. [72].

III. A DETAILED STUDY OF MODEL 5

In order to study the connection between DM and flavor physics in the above class of models, we will now focus on Model 5 in the following sections. Note that all of the models proposed in the previous section should lead to very similar results in the for the flavor and DM physics. Therefore, a detailed study of one specific model is enough to understand many of the common features in the whole class. The differences between models will show at the level of the allowed parameter space in the scans. However, the important point is to show that these are models that explain the experimental deviations. On the other hand, Model 5 is a brand new model, which deserves a careful exploration in itself.

As shown in Table V, there are three additional particles in this model: one fermion doublet $\chi_{L,R} = (\chi^0_{L,R}, \chi^-_{L,R})$ and two scalar $SU(2)_L$ singlets: Φ_l and Φ_q, in which Φ_l is electrically neutral while Φ_q has colour and an electric charge of $2/3$. We also impose a Z_2 symmetry under which all new fields are odd while the SM fields are even under Z_2. As a result, we can introduce the following Dirac mass and Yukawa couplings to the fermion χ:

$$\mathcal{L} \supset m_\chi \bar{\chi}_L \chi_R + y_{Q_i} \bar{Q}_{Li} \Phi_q \chi_R + y_{L_i} \bar{L}_{Li} \Phi_l \chi_R + \text{H.c.}, \tag{8}$$

where Q_{Li} and L_{Li} denote the left-handed quark and lepton doublets in the SM. Note that both χ^0 and $\chi^\pm$ share the same mass m_χ at tree level due to the fact that the Dirac mass term above is the sole source for both fermions.

We decompose the neutral complex scalar Φ_l into its real and imaginary components as $\Phi_l = (S + iA)/\sqrt{2}$. The scalar potential can be written as follows:

$$\begin{aligned} V(H, \Phi_q, \Phi_l) = {} & -\mu_H^2 |H|^2 + \mu_{\Phi_l}^2 |\Phi_l|^2 + \mu_{\Phi_q}^2 |\Phi_q|^2 + \frac{\mu'^2_{\Phi_l}}{2} (\Phi_l^2 + \Phi_l^{*2}) \\ & + \lambda_H |H|^4 + \lambda_{\Phi_q} |\Phi_q|^4 + \lambda_{\Phi_l} |\Phi_l|^4 + \lambda_{H\Phi_q} |H|^2 |\Phi_q|^2 + \lambda_{H\Phi_l} |H|^2 |\Phi_l|^2 + \lambda_{\Phi_q \Phi_l} |\Phi_q|^2 |\Phi_l|^2 \\ & + \frac{\lambda'_{\Phi_l}}{4} (\Phi_l^2 + \Phi_l^{*2})^2 + \frac{\lambda'_{\Phi_q \Phi_l}}{2} |\Phi_q|^2 (\Phi_l^2 + \Phi_l^{*2}) + \frac{\lambda'_{H\Phi_l}}{2} |H|^2 (\Phi_l^2 + \Phi_l^{*2}). \end{aligned} \tag{9}$$

After electroweak symmetry breaking, the SM Higgs doublet H acquires its vacuum expectation value $v_H = \sqrt{\mu_H^2/\lambda_H}$ and the scalar particles mass spectrum is given by

$$\begin{aligned} & m_h^2 = 2\lambda_H v_H^2, \qquad m_{\Phi_q}^2 = \mu_{\Phi_q}^2 + \frac{1}{2}\lambda_{H\Phi_q} v_H^2, \\ & m_S^2 = \mu_{\Phi_l}^2 + \mu'^2_{\Phi_l} + \frac{1}{2}(\lambda_{H\Phi_l} + \lambda'_{H\Phi_l}) v_H^2, \qquad m_A^2 = \mu_{\Phi_l}^2 - \mu'^2_{\Phi_l} + \frac{1}{2}(\lambda_{H\Phi_l} - \lambda'_{H\Phi_l}) v_H^2, \end{aligned} \tag{10}$$

where h is the only component left in the SM Higgs doublet as $H = (0, (v_H + h)/\sqrt{2})^T$ in the unitary gauge. As argued in Sec. II, there are two potential DM candidates in this model: the neutral component χ^0 in the fermionic doublet and the neutral scalar S or the pseudoscalar A in the scalar singlet Φ_l. However, the fermionic candidate χ^0 has a very large DM-nucleon scattering cross section due to the tree-level Z mediation. In order to avoid the stringent experimental constraints from DM direct searches, such as XENON1T [76], the fermionic DM mass should be pushed to be of $\mathcal{O}(\mathrm{TeV})$. On the other hand, if all new particles are above 1 TeV, the loop contributions to $b\to s\mu^+\mu^-$ and Δa_μ are too small to solve the associated flavor anomalies, even if we tune the Yukawa couplings in Eq. (8) to their perturbative limits $\sqrt{4\pi}$ [71]. Thus, we will not consider the fermionic DM candidate χ^0 and concentrate on the physics of the (pseudo)scalar DM $S(A)$. We should note that the DM and flavor phenomenology of this model are exactly the same for either S or A. Hence, without loss of generality, we assume that $m_S < m_A$ so that S comprises the whole DM density. According to Eq. (10), it implies the following relation $\mu'^2_{\Phi_l}+\frac{1}{2}\lambda'_{H\Phi_l}v_H^2<0$.

We can also rewrite the Yukawa interactions in Eq. (8) relevant to solve the B decay anomaly as follows:

$$\begin{aligned}\mathcal{L}\supset\, & y_{d_i}(\bar{u}_{Lj}V_{ji}\chi_R^0+\bar{d}_{Li}\chi_R^-)\Phi_q\\ &+\frac{y_{e_i}}{\sqrt{2}}(S+iA)(\bar{\nu}_{Lj}U_{ji}\chi_R^0+\bar{e}_{Li}\chi_R^-)+\mathrm{H.c.}\end{aligned}\tag{11}$$

where we have defined the Yukawa couplings $y_{d_i(e_i)}$ which are obtained from $y_{Q_i(L_i)}$ by transforming the quarks and leptons into their mass eigenstates, and the matrix V and U are the Cabibbo-Kobayashi-Maskawa (CKM) and the Pontecorvo-Maki-Nakagawa-Sakata (PMNS) matrices, respectively. In order to suppress the strong flavor constraints on the first-generation quarks and leptons and to keep our discussion as simple as possible, we only allow these Z_2-odd particles to couple to quarks of the last two generations and the second-generation leptons. In other words, we only take y_b, y_s, and y_μ to be nonzero.

Since we have included several Z_2-odd particles to the particle spectrum, one might be concerned that they would induce corrections to the EW oblique parameters S, T and U [77,78], and, in turn, destroy the successful EW precision test established in the SM. However, according to their definitions of these EW oblique parameters, both $SU(2)_L$ singlets Φ_q and $\Phi_l=(S+iA)/\sqrt{2}$ cannot contribute. On the other hand, since both components in the doublet vectorlike fermion χ share the same mass at tree level, their total contributions to S, T and U vanish at the one-loop order. These corrections will only appear at the two-loop order. Therefore, the model studied here is free of the constraints from the EW precision test at one-loop, which will not be considered in our set of constraints.

IV. FLAVOR PHENOMENOLOGY

In this section we discuss the NP contributions to the various flavor observables in model 5. We will present the relevant analytic expressions used to perform the numerical scan presented in Sec. VI.

A. $(g-2)_\mu$

The general amplitude of photon interactions with a charged particle can be written as

$$\begin{aligned}\bar{u}(p')e\Gamma_\mu u(p)=\bar{u}(p')\Big[&e\gamma_\mu F_1(q^2)\\ &+\frac{ie\sigma_{\mu\nu}q^\nu}{2m_f}F_2(q^2)+\cdots\Big]u(p),\end{aligned}\tag{12}$$

in which the photon momentum is defined as to flow into the vertex. The magnetic moment of muon is defined as $a_\mu=F_2(0)$. As mentioned in the Introduction, there is a long-standing discrepancy between the SM theoretical and experimental values of a_μ given in Eq. (5) [39,40]. We hope to explain the anomalous magnetic moment of muon, i.e., $(g-2)_\mu$, within our model, where the leading-order contribution is provided by the one-loop diagrams enclosed by the negatively charged fermion χ_R and the neutral scalars H or A. According to Ref. [34], the NP contribution is

$$\begin{aligned}\Delta a_\mu &=\frac{m_\mu^2|y_\mu|^2}{8\pi^2m_\chi^2}\left(-\frac{1}{2}Q_\chi\right)[\tilde{F}_7(x_S)+\tilde{F}_7(x_A)]\\ &=\frac{m_\mu^2|y_\mu|^2}{16\pi^2m_\chi^2}[\tilde{F}_7(x_S)+\tilde{F}_7(x_A)],\end{aligned}\tag{13}$$

where

$$\tilde{F}_7(x)=\frac{1-6x+3x^2+2x^3-6x^2\ln x}{12(1-x)^4},\tag{14}$$

and $x_{S(A)}=m_{S(A)}^2/m_\chi^2$.

B. $B\to K^{(*)}\mu^+\mu^-$

It is easy to see that the anomalies in B meson decays can be explained microscopically by the flavor-changing neutral current process $b\to s\mu^+\mu^-$. In the present model, we can generate the following relevant effective Hamiltonian for $b\to s\mu^+\mu^-$ [79,80]:

$$\mathcal{H}_{\mathrm{eff}}=-\frac{4G_F}{\sqrt{2}}V_{tb}V_{ts}^*(C_9^{\mathrm{NP}}\mathcal{O}_9+C_{10}^{\mathrm{NP}}\mathcal{O}_{10}),\tag{15}$$

where

$$\mathcal{O}_9=\frac{\alpha}{4\pi}[\bar{s}\gamma^\nu P_Lb][\bar{\mu}\gamma_\nu\mu],\qquad \mathcal{O}_{10}=\frac{\alpha}{4\pi}[\bar{s}\gamma^\nu P_Lb][\bar{\mu}\gamma_\nu\gamma^5\mu],\tag{16}$$

in which α is the fine structure constant of the electromagnetic interaction.

In our model, there are three kind of diagrams contributing to these two operators: box diagrams as well as γ- and Z-penguin diagrams. However, as shown in Ref. [34], the Z-penguin diagrams are suppressed by the factor m_b^2/m_Z^2 and can therefore be neglected. In what follows, we only consider the box and γ-penguin contributions.

The box diagrams in this model are shown in Fig. 1 with the original complex scalar Φ_l replaced by its real and imaginary components, S and A. They give new contributions to the Wilson coefficient $C_{9,10}^{\rm NP}$ as follows [34]:

$$C_9^{\rm box} = -C_{10}^{\rm box} = \mathcal{N}\frac{y_s y_b^* |y_\mu|^2}{64\pi\alpha m_\chi^2}[F(x_{\Phi_q}, x_S) + F(x_{\Phi_q}, x_A)], \tag{17}$$

where $x_{\Phi_q,S,A} \equiv m_{\Phi_q,S,A}^2/m_\chi^2$ and $\mathcal{N}^{-1} = 4G_F V_{tb}V_{ts}^*/\sqrt{2}$. The function $F(x,y)$ is defined as

$$F(x,y) = \frac{1}{(1-x)(1-y)} + \frac{x^2 \ln x}{(1-x)^2(x-y)} + \frac{y^2 \ln y}{(1-y)^2(y-x)}. \tag{18}$$

There are two γ-penguin diagrams differentiated by the internal lines from which the photon is emitted, since both loop particles, Φ_q and χ^-, are electrically charged. Also, note that these two diagrams only generate the effective operator $\mathcal{O}_9$, with the corresponding Wilson coefficient given by[1]

$$C_9^\gamma = \mathcal{N}\frac{y_s y_b^*}{m_\chi^2}[Q_{\Phi_q}F_9(x_{\Phi_q}) - Q_\chi G_9(x_{\Phi_q})], \tag{19}$$

where the functions $F_9(x)$ and $G_9(x)$ are defined by [34]

$$F_9(x) = \frac{-2x^3 + 9x^2 - 18x + 11 + 6\ln x}{36(1-x)^4},$$
$$G_9(x) = \frac{7 - 36x + 45x^2 - 16x^3 + 6(2x-3)x^2 \ln x}{36(1-x)^4}. \tag{20}$$

However, after numerical calculations of the box and γ-penguin diagrams, we find that the NP amplitude of $b \to s\mu^+\mu^-$ is always dominated by the box diagrams in our model, i.e., $C_9^{\rm NP} = C_9^{\rm box} + C_9^\gamma \simeq C_9^{\rm box} = -C_{10}^{\rm box} = -C_{10}^{\rm NP}$. This indicates that the relevant operator in our model reduces to a single left-handed one of the form $(\alpha/4\pi)[\bar{s}\gamma^\nu P_L b][\bar{\mu}\gamma_\nu(1-\gamma_5)\mu]$, which has been widely investigated in the literature [30,81–95] because evidence for $R(K^{(*)})$ anomalies was observed in 2014. More recently, this scenario has been revisited in Ref. [96] by fitting this single operator with the latest $b \to s\mu^+\mu^-$ and $R(K^{(*)})$ data measured by the LHCb and Belle Collaborations. The best fitted value of the Wilson coefficient is given by $C_9^{\rm NP} = -C_{10}^{\rm NP} = -0.53 \pm 0,08$, with the improvement of the data fitting by 5.8σ compared with the SM predictions. In our subsequent numerical scan of the parameter space, we only keep the models which can generate the Wilson coefficient $C_9^{\rm NP} = -C_{10}^{\rm NP}$ to be within the 2σ range around its central value. Note that recent works in Refs. [91,96] have shown that the single left-handed operator cannot provide a perfect fit to the whole set of B meson decay data. In order to totally reduce the tension, one needs to consider extensions beyond this simple framework in the fits. However, we will not consider such complicated scenarios in the present work.

The rare decay process $B_s \to \mu^+\mu^-$ may play a crucial role in constraining the present scenario with $C_9^{\rm NP} = -C_{10}^{\rm NP}$. In the SM, this decay channel is induced by the box and penguin diagrams. Due to helicity suppression of this process, only the operator $\mathcal{O}_{10}$ can contribute, with the SM expression of its branching fraction given by [97]:

$$\mathcal{B}(B_s \to \mu^+\mu^-)^{\rm SM} = \tau_{B_s} f_{B_s}^2 m_{B_s}\frac{G_F^2\alpha^2}{16\pi^3}|V_{tb}V_{ts}^*|m_\mu^2|C_{10}^{\rm SM}|^2 \times \sqrt{1 - \frac{4m_\mu^2}{m_{B_s}^2}}. \tag{21}$$

where m_{B_s}, f_{B_s}, and τ_{B_s} refer to the meson B_s's mass, decay constant, and lifetime, respectively, and $C_{10}^{\rm SM}$ is the SM value to Wilson coefficient of the effective operator $\mathcal{O}_{10}$. On the other hand, our model can generate $\mathcal{O}_{10}$ via the NP box diagrams with its Wilson coefficient $C_{10}^{\rm NP}$. As a result, the NP contributions to this B_s decay process is simply given by Eq. (21) with the SM Wilson coefficient $C_{10}^{\rm SM}$ replaced by its NP one $C_{10}^{\rm NP}$ [72].

Numerically, the SM prediction of the branching ratio for $B_s \to \mu^+\mu^-$ is given by [97]

$$\mathcal{B}(B_s \to \mu^+\mu^-)^{\rm SM} = (3.65 \pm 0.23) \times 10^{-9}, \tag{22}$$

while the measurement performed by the LHCb Collaboration has given [39,98]

$$\mathcal{B}(B_s \to \mu^+\mu^-)^{\rm Exp} = (2.7^{+0.6}_{-0.5}) \times 10^{-9}, \tag{23}$$

which shows that the measurement agrees with the SM value within 1σ confidence level (CL). In the following, we will constrain our model by requiring the NP contribution to this channel to be within the 2σ CL experimentally allowed range.

C. $B_s - \bar{B}_s$ mixing

A further important constraint on the parameter space related to the $b \to s$ transition is provided by the B_s-$\bar{B}_s$ mixing. Since the NP in our model only involves the left-handed SM fermions, the contribution to B_s-$\bar{B}_s$ mixing can only arise from the following single one effective operator

[1]Compared with Eq. (3.7) in Ref. [34], our result for C_9^γ is larger by a factor of 2.

$$\mathcal{H}_{\rm eff}^{B\bar{B}} = C_{B\bar{B}} Q_1 \equiv C_{B\bar{B}} (\bar{s}_\alpha \gamma^\mu P_L b_\alpha)(\bar{s}_\beta \gamma^\mu P_L b_\beta), \tag{24}$$

where α and β denote the color indices which are contracted in each pair. The NP contribution to the above Wilson coefficient in our model is given by [34]

$$C_{B\bar{B}}^{\rm NP} = \frac{(y_s y_b^*)^2}{128\pi^2 m_\chi^2} F(x_{\Phi_q}, x_{\Phi_q}), \tag{25}$$

where

$$F(x,x) = \frac{1 - x^2 + 2x\ln x}{(1-x)^3} \tag{26}$$

is the function $F(x,y)$ defined in Eq. (18) in the limit of equal arguments.

The constraint is imposed on the mass difference ΔM_s between the two neutral meson states, B_s and $\bar{B}_s$. According to Ref. [35], we can represent the constraint in terms of the ratio of the experimental value of the B_s meson mass difference $\Delta M_s^{\rm exp}$ with its SM counterpart $\Delta M_s^{\rm SM}$ as follows [35]:

$$R_{\Delta M_s} = \frac{\Delta M_s^{\rm exp}}{\Delta M_s^{\rm SM}} - 1 = -0.09 \pm 0.08, \quad \text{at } 1\sigma \text{ C.L.}, \tag{27}$$

where, in order to compute the SM result, we have used the value of the matrix element $\langle \bar{B}_s | Q_1(\mu_b) | B_s \rangle$ obtained from a $N_f = 2+1$ lattice simulation in Ref. [99], which is consistent with the $N_f = 2$ result in Ref. [100], the sum rules calculation in Ref. [101], and the most recent FLAG-2019 lattice average value in Ref. [102]. Here $Q_1(\mu_b)$ is the effective operator defined in Eq. (24) at the scale μ_b. If we further identify $\Delta M_s^{\rm exp}$ as the total contribution to the B_s-$\bar{B}_s$ mixing mass difference, we can write the quantity $R_{\Delta M_s}$ in terms of the NP and SM Wilson coefficients as follows [35,103]:

$$R_{\Delta M_s} = \left| 1 + \frac{0.8 C_{B\bar{B}}^{\rm NP}(\mu_H)}{C_{B\bar{B}}^{\rm SM}(\mu_b)} \right| - 1, \tag{28}$$

where $C_{B\bar{B}}^{\rm NP}(\mu_H)$ is the NP Wilson coefficient defined at a high-energy scale of $\mu_H = 1$ TeV, and $C_{B\bar{B}}^{\rm SM} \simeq 7.2 \times 10^{-11}$ GeV^{-2} is the corresponding SM value defined at the scale μ_b computed by employing the results in Ref. [99]. Also, the factor 0.8 is caused by the renormalization group running and the operator mixing as the scale decreases from μ_H to μ_b.

Note that it is easily seen from Eq. (27) that there is a little tension between experimental measurements and the SM prediction as pointed out in Refs. [104,105]. However, we did not try to solve this tension in the present paper. Rather, we will constrain $C_{B\bar{B}}^{\rm NP}$ by requiring the $R_{\Delta M_s}$ to lie in its 2σ confidence interval.

D. $b \to s\gamma$

Another strong constraints on our model arises from the $b \to s\gamma$ processes. The relevant effective Hamiltonian is given by [34]

$$\mathcal{H}_{\rm eff}^{\gamma} = -\frac{4G_F}{\sqrt{2}} V_{tb} V_{ts}^* (C_7 \mathcal{O}_7 + C_8 \mathcal{O}_8), \tag{29}$$

with

$$\begin{aligned} \mathcal{O}_7 &= \frac{e}{16\pi^2} m_b \bar{s} \sigma^{\mu\nu} P_R b F_{\mu\nu}, \\ \mathcal{O}_8 &= \frac{g_s}{16\pi^2} m_b \bar{s}_\alpha \sigma^{\mu\nu} P_R T^a_{\alpha\beta} b_\beta G^a_{\mu\nu}, \end{aligned} \tag{30}$$

where $F_{\mu\nu}$ and $G^a_{\mu\nu}$ stand for the field strength tensors for photons and gluons, respectively. Note that even though $\mathcal{O}_8$ cannot give direct contributions to $b \to s\gamma$, it would affect the final result via its mixing with $\mathcal{O}_7$ as the renormalization scale decreases.

In our model, the leading-order contribution to $b \to s\gamma$ is given at one-loop order, leading to the following Wilson coefficients for $\mathcal{O}_7$ and $\mathcal{O}_8$ [34]

$$\begin{aligned} C_7 &= \mathcal{N} \frac{y_s y_b^*}{2m_\chi^2} [Q_{\Phi_q} F_7(x_{\Phi_q}) - Q_\chi \tilde{F}_7(x_{\Phi_q})], \\ C_8 &= \mathcal{N} \frac{y_s y_b^*}{2m_\chi^2} F_7(x_{\Phi_q}), \end{aligned} \tag{31}$$

where

$$F_7(x) = \frac{2 + 3x - 6x^2 + x^3 + 6x\ln x}{12(1-x)^4}, \tag{32}$$

while $\tilde{F}_7(x)$ has been shown in Eq. (14).

Currently, the most precise experimental measurement on the branching ratio of $b \to s\gamma$ is given by the HFAG Collaboration [106]:

$$\mathcal{B}^{\rm exp}(b \to s\gamma) = (3.32 \pm 0.15) \times 10^{-4}, \tag{33}$$

while the SM prediction of the branching ratio for this process is [107,108]

$$\mathcal{B}^{\rm SM}(b \to s\gamma) = (3.36 \pm 0.23) \times 10^{-4}, \tag{34}$$

which shows a good agreement between the experiments and theoretical calculations. In order to impose the $b \to s\gamma$ constraint on our model, we follow Ref. [34,35] to define

$$R_{s\to\gamma} = \frac{\mathcal{B}^{\rm tot}(b \to s\gamma)}{\mathcal{B}^{\rm SM}(b \to s\gamma)} - 1 = -2.87(C_7 + 0.19 C_8), \tag{35}$$

where $\mathcal{B}^{\rm tot}(b \to s\gamma)$ refers to the total branching ratio of $b \to s\gamma$ in our model including the NP contribution.

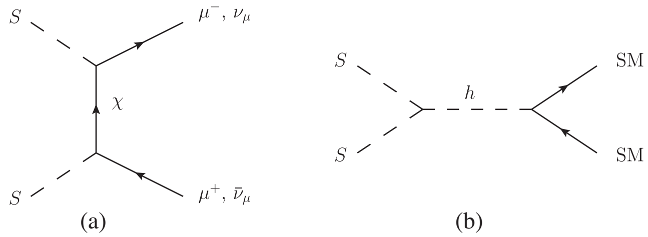

FIG. 2. Feynman diagrams for DM S annihilations: (a) $SS \to \mu^+\mu^-$ via the χ mediation; (b) $SS \to \mathrm{SM}\,\mathrm{SM}$ via the SM-like Higgs mediation in which "SM" represents all massive SM particles.

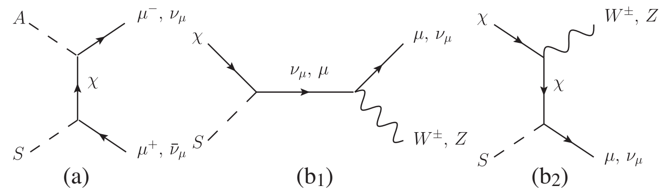

FIG. 3. Illustration of Feynman diagrams for (a) SA and (b) $S\chi$ co-annihilation processes relevant to the determination of the DM relic abundance.

Here the combination $C_7 + 0.19C_8$ accounts for the mixing effect between effective operators $\mathcal{O}_7$ and $\mathcal{O}_8$ due to the renormalization group running from QCD calculations [107,108]. On the other hand, by appropriately combining the experimental and theoretical errors in Eqs. (33) and (34), it can be shown $R_{b\to s\gamma} = (-0.7 \pm 8.2) \times 10^{-2}$ at the 2σ confidence level [35], which can be transformed into

$$|C_7 + 0.19C_8| \lesssim 0.06 \quad \text{at } 2\sigma \text{ C.L..} \tag{36}$$

V. DARK MATTER PHENOMENOLOGY

As discussed, the neutral scalar component S contained in the singlet Φ_l is the lightest Z_2-odd particle. It is therefore stable and can play the role of DM candidate. In what follows, we will discuss the DM phenomenology, by exploring the DM relic density and constraints from DM searches.

A. Dark matter relic density

Since S is the only DM candidate it should reproduce the observed DM relic abundance. Currently, the most accurate measurement of this important quantity is provided by the Planck Collaboration with $\Omega_{\mathrm{DM}}h^2 = 0.1199 \pm 0.0022$ [46]. Here we assume that the DM relic density is generated by the ordinary freeze-out mechanism, so that the relic abundance of S can be determined by solving the following Boltzmann equation:

$$\frac{dn_S}{dt} + 3Hn_S = -\langle\sigma v\rangle(n_S^2 - n_S^{\mathrm{eq}\,2}), \tag{37}$$

where n_S denotes the number density of S with n^{eq} as its corresponding equilibrium value, H is the Hubble parameter and $\langle\sigma v\rangle$ refers to the thermal average of the DM annihilation cross section times the relative velocity' v.

The two main classes of DM annihilation processes crucial to determine the DM relic abundance are presented in Fig. 2. On the left we show S pair annihilation into a $\mu^+\mu^-$ ($\nu_\mu\bar{\nu}_\mu$) pair via the t- and u-channel χ^- (χ^0) mediation. On the right, the s-channel annihilation mode mediated by the SM Higgs h is shown. The process $SS \to \mu^+\mu^-$ is dominated by the d-wave contribution in the zero muon mass limit, with its cross section given by

$$\begin{aligned}\langle\sigma v\rangle_{SS\to\mu^+\mu^-} &= \frac{|y_\mu|^4}{240\pi}\frac{m_S^6}{(m_\chi^2 + m_S^2)^4}\langle v^4\rangle \\ &= \frac{|y_\mu|^4}{128\pi}\frac{m_S^6}{(m_\chi^2 + m_S^2)^4}\frac{1}{x^2},\end{aligned} \tag{38}$$

where the angle bracket refers to taking the thermal average of the corresponding quantity, and we have used the formula $\langle v^4\rangle = 15/(8x^2)$ for the nonrelativistic Boltzmann distribution [109] in which $x^{-1} \equiv T/m_S \approx 1/25$ with T being the plasma temperature at the DM freeze-out time in the Universe. The cross section for the process $SS \to \nu_\mu\bar{\nu}_\mu$ is also given by Eq. (38). For the DM annihilation processes with the h mediation, the cross sections for different final states are all proportional to the Higgs portal coupling $(\lambda_{H\Phi_l} + \lambda'_{H\Phi_l})$, which are strongly constrained by DM direct detection results. Using several benchmark sets of parameters we found that when the mass difference between S and $A(\chi)$ is comparable to or smaller than the temperature of the Universe, the number density of A (χ) is abundant at the DM freeze-out, and the coannihilation $SA(S\chi)$ channels illustrated in Fig. 3 are still active in determining the model prediction of the DM relic density.

In our work, we numerically solve the Boltzmann equation in Eq. (37) by taking advantage of the modified MICROMEGAS v4.3.5 code [110,111] which takes all possible coannihilation channels into account. As an example of our numerical calculation, we show in Fig. 4 the variation of the DM relic abundance as a function of the DM mass m_S for different leptonic Yukawa couplings $y_\mu = 0.5$, 1.0, and $\sqrt{4\pi}$ with the last value corresponding to the perturbative limit. We have fixed the relevant parameters to be $m_{\Phi_q} = 2$ TeV, $\lambda_{H\Phi_l} = \lambda'_{H\Phi_l} = 5 \times 10^{-3}$ and $y_s = -y_b = 0.1$, as well as the mass differences to be $\Delta m_{AS} \equiv m_A - m_S = 60$ GeV and $\Delta m_{AS} \equiv m_A - m_S = 250$ GeV. From Fig. 4, it is seen that when $(\lambda_{H\Phi_l} + \lambda'_{H\Phi_l})$ is 10^{-2} and y_μ is small, i.e., $y_\mu \lesssim 0.5$, the DM relic abundance is only satisfied in the region near the SM Higgs resonance $m_S \simeq m_h/2$, and the dominant DM annihilation proceeds via the s-channel SM Higgs mediation. When y_μ

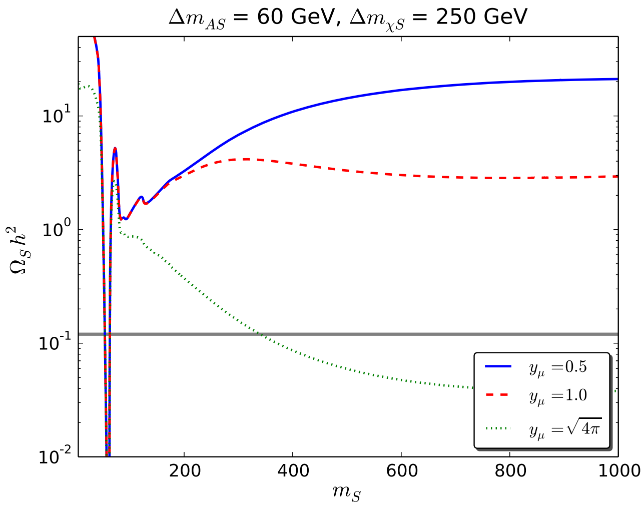

FIG. 4. The DM S relic density as a function of the DM mass m_S. Here we fix the difference between the particle A (χ) mass and the DM mass to be $\Delta m_{AS} \equiv m_A - m_S = 60$ GeV ($\Delta m_{\chi S} \equiv m_\chi - m_S = 250$ GeV). Other relevant parameters are fixed to be $m_{\Phi_q} = 2000$ GeV, $\lambda_{H\Phi_l} = \lambda'_{H\Phi_l} = 5 \times 10^{-3}$, and $y_s = -y_b = 0.1$.

is increased to be around 1, the d-wave suppressed process $SS \to \mu^+\mu^-$, $\nu_\mu\bar{\nu}_\mu$ induced by the new Yukawa interactions begins to be comparable to and even dominant over the SM Higgs mediated diagrams in the high DM mass region. However, the total DM annihilation cross section is still insufficient to lower the DM relic abundance to its experimentally allowed values. Finally, when y_μ becomes even larger, up to the perturbative limit $\sqrt{4\pi}$, a second allowed DM region appears in the high DM mass region where the t- and u-channel S annihilations into leptons dominate the DM freeze-out, over the whole range of DM masses except for the Higgs resonance region.

B. Constraints from dark matter direct detection and Higgs invisible decays

In this subsection, we will focus on the experimental constraints from various DM searches. Let us begin by discussing DM direct detection, which may place severe constraints on the spin-independent DM-nucleon scattering. In the present model, the dominant DM direct detection signal arises through the tree-level diagram with t-channel SM-like Higgs mediation, leading to the following DM-nucleon scattering cross section

$$\sigma(SN \to SN) = \frac{(\lambda_{H\Phi_l} + \lambda'_{H\Phi_l})^2}{4\pi} \frac{f_N^2 m_N^2 \mu_{SN}^2}{m_S^2 m_h^4}, \quad (39)$$

where $f_N \simeq 0.3$ denotes the effective Higgs-nucleon coupling [112–114], m_N is the nucleon mass, and $\mu_{SN} \equiv m_S m_N/(m_S + m_N)$ is the reduced mass of the DM-nucleon system. At present, the best experimental upper bound on the DM direct detection cross section for a mass above 6 GeV is provided by the XENON1T experiment [76], which will be taken into account in our scan.

Collider searches impose further restrictions on dark matter. These are particularly relevant when $m_S < m_h/2$ because the DM particle S is subject to the constraint from the SM-like Higgs boson invisible decay into an S pair. The invisible decay width in our model is given by

$$\Gamma(h \to SS) = \frac{(\lambda_{H\Phi_l} + \lambda'_{H\Phi_l})^2 v_H^2}{32\pi m_h} \sqrt{1 - \frac{4m_S^2}{m_h^2}}. \quad (40)$$

Currently, the upper bound on this process is provided by LHC with $\mathcal{B}(h \to SS) \le 0.24$ [39]. Note that both the DM direct detection signal in Eq. (39) and the SM-like Higgs invisible decay in Eq. (40) only depend on two parameters: m_S and $(\lambda_{H\Phi_l} + \lambda'_{H\Phi_l})$. As a result, the constraint from the Higgs invisible decay is always weaker than that of DM direct detection in the parameter space of interest.

VI. RESULTS

In this section we discuss the results obtained by analyzing the flavor and DM physics constraints in our model. We perform a multiparameter scan to find out the common parameter regions that can satisfy all relevant flavor constraints: $R(K^{(*)})$, $\mathcal{B}(B_s \to \mu^+\mu^-)$, B_s-$\bar{B}_s$ mixings, $b \to s\gamma$, the muon anomalous magnetic moment Δa_μ, and the DM constraints, where the latter means both the correct DM relic abundance and the bounds on the direct detection searches. In order to simplify our analysis, we make the following restrictions of our parameter space. As shown in the formulas related to the B_s meson decays and the B_s-$\bar{B}_s$ mixing, only the combination $y_s y_b^*$ appears. Also, in order to solve the deficit observed in the measurements of $R(K^{(*)})$, this combination should be negative. Therefore, in our numerical scan we take y_s and y_b to be real with $y_s = -y_b/4$. Regarding DM, since the Higgs portal coupling is always of the form $(\lambda_{H\Phi_l} + \lambda'_{H\Phi})$, we take $\lambda_{H\Phi} = \lambda'_{H\Phi}$. Moreover, the singlet Φ_q can be pair produced via gluon/quark fusion at the LHC, and one of its main decay channels is an up-type quark plus a χ^0 which in turn decays into the DM particle S and a neutrino, leading to a dijet plus missing transverse energy final state, i.e., $jj + \not{E}_T$. According to a similar study in Ref. [71],[2] the lower limit on Φ_q is around 1 TeV. Therefore, in order to avoid such a strong constraint, we fix the mass of the colored scalar Φ_q to be $m_{\Phi_q} = 1.5$ TeV. Furthermore, for S

[2]Although the colored scalar Φ_q in Ref. [71] has a different electroweak quantum number from the one in the present paper, the main production channel is still through the QCD processes. Thus, the constraint on Φ_q can be directly applied in our case.

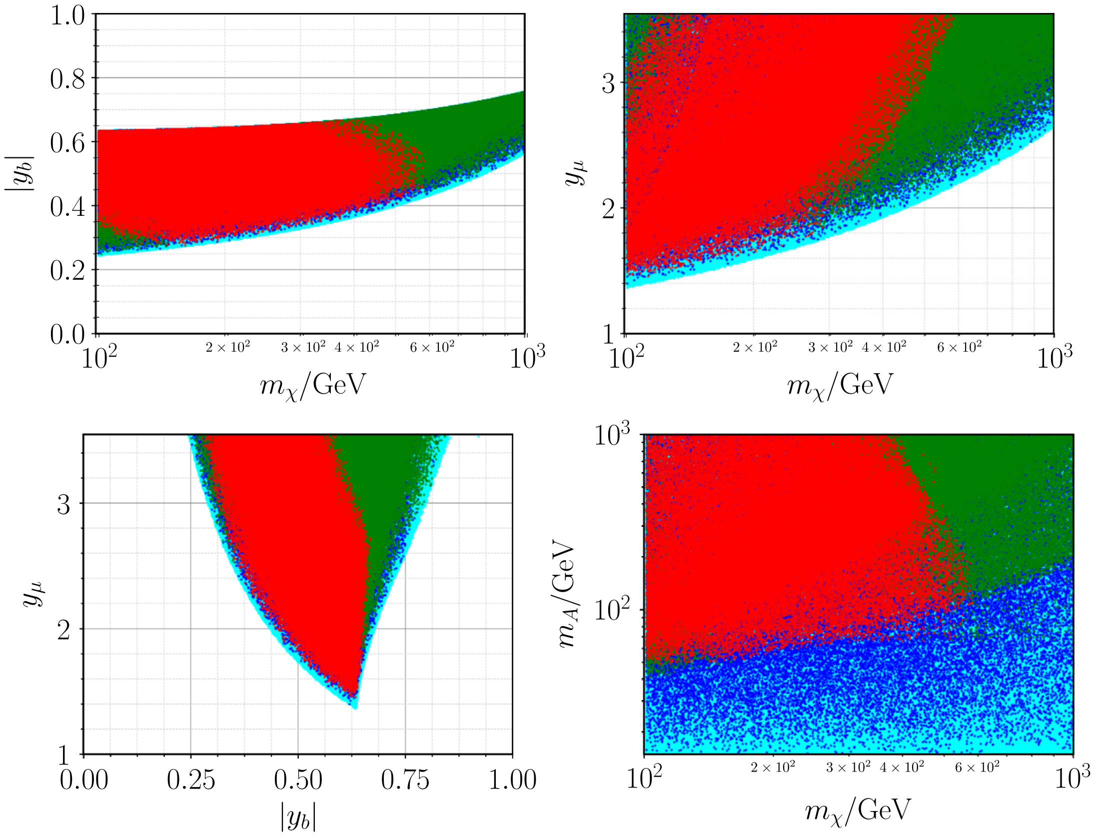

FIG. 5. Allowed parameter space projected in the planes $m_\chi - |y_b|$ (top left), $m_\chi - y_\mu$ (top right), $|y_b| - y_\mu$ (bottom left), and $m_\chi - m_A$ (bottom right). In the scan, we have fixed $m_{\Phi_q} = 1.5$ TeV and chosen $y_s = -y_b/4$ and $\lambda_{H\Phi_l} = \lambda'_{H\Phi_l}$. All points satisfy the constraints from the nonanomalous B-physics results. We shown in cyan the points that explain $R(K^{(*)})$; the blue points explain $R(K^{(*)})$ and the DM relic density; the green points explain the B anomalies and DM relic density while satisfying all constraints except the muon $(g-2)$; red points satisfy all constraints.

to be the DM candidate, we require all other particles in the dark sector, including A and χ, to be heavier than S by at least 10 GeV, but all these particles should be lighter than 1 TeV. A further constraint coming from LEP searches for unstable heavy vectorlike charged leptons [115], which sets a lower limit on the mass of the charged fermion $\chi^\pm$ of 101.2 GeV. We also impose this limit in our scan. For dimensionless couplings, we allow $(\lambda_{H\Phi} + \lambda'_{H\Phi}) \leq 1$, $|y_b| \leq 1$, and $0 \leq y_\mu \leq \sqrt{4\pi}$.

In our numerical study, we perform a random scan of more than 10^9 benchmark model points over the whole parameter space with the restrictions listed above. The final scanning results are shown in Figs. 5 and 6. First, all the colored points explain the $R(K^{(*)})$ associated anomalies while satisfying the $\mathcal{B}(B_s \to \mu^+\mu^-)$ and $b \to s\gamma$ data within their 2σ confidence intervals. Second, when taking into account the observed DM relic abundance within 2σ CL range, the cyan colored points are excluded. The blue points correspond to those models which cannot satisfy the constraints from DM searches. In particular, the dominant experimental bound comes from the DM direct detection experiment XENON1T as evident from the lower right plot of Fig. 6. Finally, the green points represent the models that are not allowed by the muon $(g-2)$ data within its 3σ range, while the red region is the common parameter space which can explain all the possible flavor and DM observations at the same time.

From Fig. 5, it is clear that the B meson decay data alone limits the dimensionless Yukawa coupling $|y_b|$ to be within the strip around 0.6, and y_μ to be greater than 1.38. The constraints from DM phenomenology, such as the DM relic density and direct detection searches, do not have a major impact on the parameter space, as can be seen by comparing the regions with cyan and blue points. Still, these DM constraints indeed limit the pseudoscalar meson mass to $m_A \gtrsim 50$ GeV. On the other hand, the inclusion of the muon $(g-2)$ data greatly reduces the allowed parameter space, with $0.25 \lesssim |y_b| \lesssim 0.65$, $1.4 \lesssim y_\mu \lesssim \sqrt{4\pi}$ and $m_\chi \lesssim 600$ GeV. This result is understandable, since the 3σ difference between the SM theoretical and experimental values of Δa_μ requires a mild suppression of the NP contribution in Eq. (13) forcing a not too large value of m_χ.

In Fig. 6, we show the same data points now in projections relevant to the DM physics. From these four

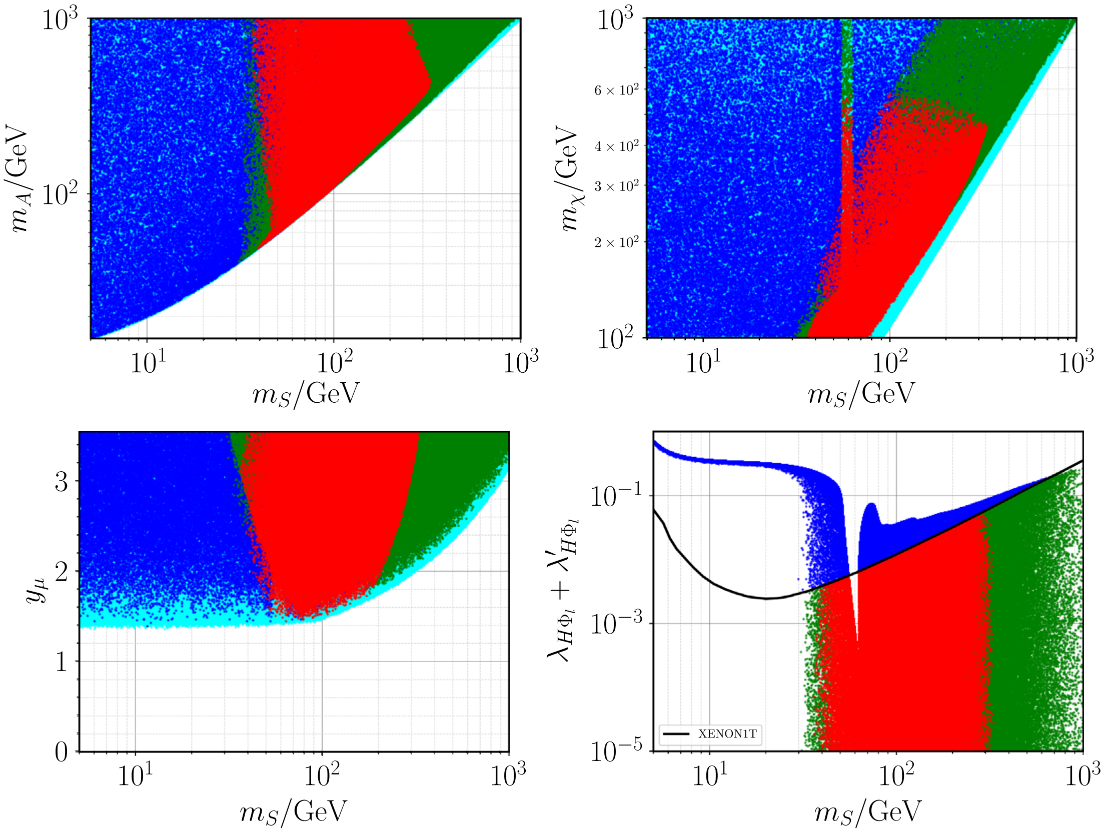

FIG. 6. Allowed parameter space projected in the planes $m_S - m_A$ (top left), $m_S - m_\chi$ (top right), $m_S - y_\mu$ (bottom left), and $m_S - (\lambda_{H\Phi_l} + \lambda'_{H\Phi_l})$ (bottom right). Other parameters are fixed as in Fig. 5.

plots, it is evident that the DM mass m_S is confined to be in the range from about 30 GeV to 350 GeV, mainly due to the constraints from DM direct detections and to the muon $(g-2)$ anomaly. Moreover, the m_S-m_χ plot (the upper-right plot) shows an interesting feature: there are two distinct regions in the allowed parameter space (red points) corresponding to the two DM dominant freeze-out channels. The first one lies around the Higgs resonance $m_S \approx m_h/2$, meaning that the dominant DM annihilation at freeze-out is through the SM-like Higgs-mediated s-channel. Note that this channel is insensitive to the mass of χ that extends to 600 GeV which is the aforementioned muon $(g-2)$ limit on m_χ. The other region starts at $m_\chi = 101.2$ GeV, where the DM mass lies in range $m_S \in [30\ \text{GeV}, 80\ \text{GeV}]$, and ends at $m_\chi \sim 600$ GeV corresponding to the DM mass range $m_S \in [140\ \text{GeV}, 350\ \text{GeV}]$. In this region there is a positive correlation between m_S and m_χ dictated by Eq. (38) for the t- and u-channel process $SS \to \mu^+\mu^-$. The bottom-right plot in the $m_S - (\lambda_{H\Phi_l} + \lambda'_{H\Phi_l})$ plane shows that the upper boundary of the colored region represents the largest value of the Higgs portal coupling $(\lambda_{H\Phi_l} + \lambda'_{H\Phi_l})$ with the correct DM relic abundance, corresponding to the cases with the Higgs-mediated process dominates over the DM annihilation during the freeze-out. The points below the boundary, beginning at around 30 GeV, are the ones where χ-mediated process $SS \to \mu^+\mu^-$ is the most important DM annihilation channel. As a result, we find that except for the Higgs resonance region in which the upper boundary is allowed by the XENON1T data, the dominant DM annihilation channel for the DM generation is $SS \to \mu^+\mu^-$. An important consequence of this result is that DM indirect detection searches [116] are not expected to give any useful constraint to the present model, since the dominant DM annihilation cross section $\langle \sigma v \rangle_{SS\to\mu^+\mu^-}$ is d-wave suppressed by its strong velocity dependence.

We finalize this section by noting that the choices $m_{\Phi_q} = 1.5$ TeV and chosen $y_s = -y_b/4$, when relaxed do not lead to any significant changes in the allowed parameter points that satisfy all constraints and explain all anomalies.

VII. CONCLUSION AND DISCUSSION

In the present work, we have explored a new class of particle physics solutions to lepton flavor universality violation observed in the decay $b \to s\mu^+\mu^-$ by the LHCb and Belle Collaborations. At the same time we wanted a model with a good DM candidate and that would solve the muon $(g-2)$ anomaly. In order to achieve this goal, we have listed several simple extensions of the model in

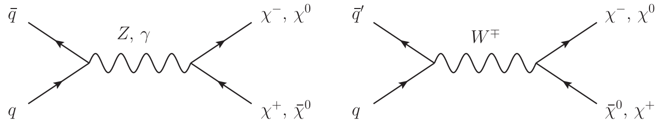

FIG. 7. Feynman diagrams for pair production of vectorlike fermions χ.

Ref. [71] by restricting the new particle's $SU(2)_L$ representations to be either singlet, doublet or triplet and with $U(1)_Y$ hypercharges such that the electric charges of the vectorlike fermion are 0 or ± 1. For each model we have identified the possible DM candidates. We have thoroughly studied the flavor and DM phenomenology in one of the most promising models in this list, in which we introduce a $SU(2)_L$ doublet vectorlike fermion χ and two complex scalar singlets, Φ_q and Φ_l, the former is an $SU(3)_c$ triplet while the latter is colorless. As a result, the $R(K^{(*)})$ anomalies related to the B meson decays can be solved by one-loop NP contributions, and the DM candidate can be the scalar component S contained in Φ_l. By performing a random scan over the whole parameter space of physical interest, we have found that the combination of the XENON1T and Δa_μ data prefer a rather light DM candidate with its mass $m_S \in [30\text{ GeV}, 350\text{ GeV}]$. Moreover, the mass of the vectorlike fermionic mediator χ is restricted to be relatively light $m_\chi \lesssim 600$ GeV, and the Yukawa couplings should be sizeable with $y_\mu \gtrsim 1.4$ and $|y_b| \sim 0.6$.

Finally, we will briefly discuss possible collider searches of this model at the LHC. Since all new particles are Z_2-odd, ATLAS and CMS strategy should be to search for final states with leptons and jets plus DM particles, which are usually identified as the missing transverse energy $\not{E}_T$. One possible signal is vectorlike lepton production mediated by $W^\pm$, Z, or γ, as illustrated in Fig. 7. The decay of $\chi^\pm$ (χ^0) leads to the final states of $\mu^\pm S$ ($\nu_\mu S$).[3] So we can consider the following LHC signals:

$$\begin{aligned} pp &\to \chi^+\chi^- \to \mu^+\mu^- + \not{E}_T, \\ pp &\to \chi^\pm\chi^0 \to \mu^\pm + \not{E}_T. \end{aligned} \tag{41}$$

The cross sections for χ pair production at the 14 TeV LHC are shown in Table IX. From this table, if $\chi^\pm$ decays dominantly into $\mu^\pm S$, we can easily observe these two signals at the present LHC run, and even more at the future LHC High Luminosity run with its 3000 fb^{-1} integrated luminosity. Note that the above two signatures have been already investigated in the literature. In Ref. [71] pair production of an $SU(2)_L$ doublet scalar with $Y = -1/2$ was studied. The Feynamn diagrams are almost the same as in Fig. 7 with the fermion χ replaced by its scalar counterpart. Using ATLAS data [117] and a leptonic Yukawa coupling equal to 2, the DM candidate lighter than 30 GeV was excluded. Taking this Yukawa coupling to its perturbative limit $\sqrt{4\pi}$, the lower bound on the DM mass decreased to about 13 GeV. Since collider constraints on such channels are insensitive to the spin of the intermediated particles, we can apply these results to our case for reference.

TABLE IX. Cross sections for χ pair productions at 14 TeV LHC.

	$m_\chi = 150$ GeV	$m_\chi = 500$ GeV
$\sigma(pp \to \chi^+\chi^-)$/pb	0.58	5.69×10^{-3}
$\sigma(pp \to \chi^-\bar{\chi}^0)$/pb	0.67	5.36×10^{-3}
$\sigma(pp \to \chi^+\chi^0)$/pb	1.27	1.43×10^{-2}

Another interesting collider signature of this model is the pair production process of the colored Z_2-odd scalar Φ_q. Note that Φ_q only couples to the second- and third-generation quarks by construction and that the dominant contribution to $\Phi_q\Phi_q^\dagger$ production at the LHC is though the pure QCD processes shown in Fig. 8. The cross section has no dependence on the Yukawa couplings y_b or y_s. Furthermore, since there is no tree-level coupling between Φ_q and the DM candidate S, Φ_q decays dominantly through the following cascade decay chains: $\Phi_q \to q\chi \to qS\mu(qS\nu_\mu)$ with the quark q representing the second- and third-generation quarks. Therefore, possible signatures are

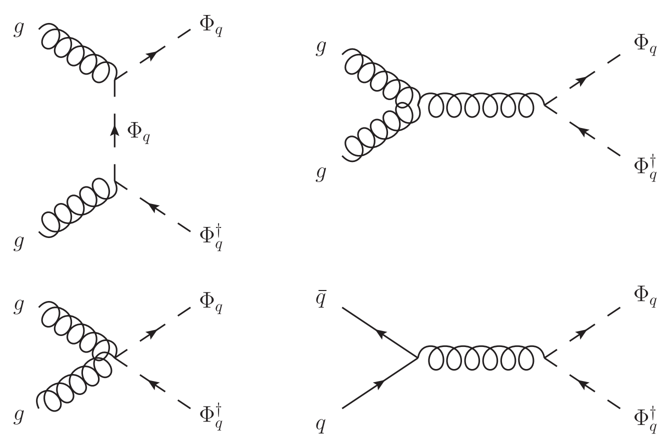

FIG. 8. Feynman diagrams for the pair production of colored scalar Φ_q.

[3] If A is lighter than χ, the decays of χ into $\mu^\pm A$ and $\nu_\mu A$ are open, and A can further decay through the three-body processes $A \to \nu_\mu\bar{\nu}_\mu S$ and $A \to \mu^+\mu^- S$, with the latter decay product observable at colliders. So here are additional LHC signatures, like $pp \to \chi^+\chi^- \to 4\mu + \not{E}_T$ or $pp \to \chi^+\chi^- \to 6\mu + \not{E}_T$. Also, the observed lepton spectra in the single-muon and dimuon channels would be modified due to the presence of A decays. However, since A is heavier than S by assumption, the phase space of the decays $\chi \to A\mu/A\nu_\mu$ would be suppressed compared with $\chi \to S\mu/S\nu_\mu$. So it is expected that the latter decay channels dominate over the former ones.

$$pp \to \Phi_q \Phi_q^\dagger \to (jj + \mu^+\mu^- + \not{E}_T)/(jj + \mu^\pm + \not{E}_T)/(jj + \not{E}_T), \quad (42)$$

where j denotes jets in the final states. A simple numerical study of the $\Phi_q \Phi_q^\dagger$ production at the LHC gives its cross section to be $\sigma(pp \to \Phi_q \Phi_q^\dagger) = 1.33 \times 10^{-4}$ pb for $m_{\Phi_q} = 1.5$ TeV. By taking into account the fact that nearly half of Φ_q goes to the final state $t(c)\bar{\chi}^0$ and the other half to $b(s)\chi^+$, it is still possible to observe the signals above at the HL run. For the dijet $+ \not{E}_T$ search, a similar scenario was carefully discussed in Ref. [71] by using recent LHC data [118], with the minor difference that the colored scalar was a $SU(2)_Y$ doublet with $Y = 1/6$ there. The general conclusion was that, for a light DM particle, the colored scalar Φ_q with $m_{\Phi_q} \lesssim 1$ TeV was excluded by the current LHC data. This result can be directly applied to our case here since the main production mechanism of the exotic colored states is the same. On the other hand, our present model predicts that the final states of $(jj + \mu^+\mu^- + \not{E}_T)$ and $(jj + \mu^\pm + \not{E}_T)$ should have almost equal cross sections as $jj + \not{E}_T$, but, due to the presence of additional muons, these two channels are more promising to be measured and probed at the LHC.

ACKNOWLEDGMENTS

D. H. and A. P. M. are supported by the Center for Research and Development in Mathematics and Applications (CIDMA) through the Portuguese Foundation for Science and Technology (FCT—Fundação para a Ciência e a Tecnologia), references No. UIDB/04106/2020 and No. UIDP/04106/2020. D. H., A. P. M., and R. S. are supported by the FCT project under Contract No. PTDC/FIS-PAR/31000/2017. D. H. is also supported by the Chinese Academy of Sciences (CAS) Hundred-Talent Program. R. S. is also supported by FCT, Contracts No. UIDB/00618/2020, No. UIDP/00618/2020, and No. CERN/FIS-PAR/0014/2019, and by the HARMONIA project [119], Contract No. UMO-2015/18/M/ST2/0518. A. P. M. is also supported by the project No. CERN/FIS-PAR/0027/2019 and by national funds (OE), through FCT, I. P., in the scope of the framework contract foreseen in the numbers 4, 5 and 6 of the article 23, of the Decree-Law 57/2016, of August 29, changed by Law 57/2017, of July 19.

[1] R. Aaij *et al.* (LHCb Collaboration), Phys. Rev. Lett. **122**, 191801 (2019).
[2] R. Aaij *et al.* (LHCb Collaboration), J. High Energy Phys. 08 (2017) 055.
[3] G. Hiller and F. Kruger, Phys. Rev. D **69**, 074020 (2004).
[4] M. Bordone, G. Isidori, and A. Pattori, Eur. Phys. J. C **76**, 440 (2016).
[5] A. Abdesselam *et al.* (Belle Collaboration), arXiv:1904.02440.
[6] A. Abdesselam *et al.* (Belle Collaboration), arXiv:1908.01848.
[7] R. Aaij *et al.* (LHCb Collaboration), J. High Energy Phys. 06 (2014) 133.
[8] R. Aaij *et al.* (LHCb Collaboration), J. High Energy Phys. 09 (2015) 179.
[9] J. T. Wei *et al.* (Belle Collaboration), Phys. Rev. Lett. **103**, 171801 (2009).
[10] T. Aaltonen *et al.* (CDF Collaboration), Phys. Rev. Lett. **108**, 081807 (2012).
[11] V. Khachatryan *et al.* (CMS Collaboration), Phys. Lett. B **753**, 424 (2016).
[12] A. Abdesselam *et al.* (Belle Collaboration), arXiv:1604.04042.
[13] J. Lees *et al.* (*BABAR* Collaboration), Phys. Rev. D **93**, 052015 (2016).
[14] R. Aaij *et al.* (LHCb Collaboration), J. High Energy Phys. 02 (2016) 104.
[15] S. Wehle *et al.* (Belle Collaboration), Phys. Rev. Lett. **118**, 111801 (2017).
[16] A. M. Sirunyan *et al.* (CMS Collaboration), Phys. Lett. B **781**, 517 (2018).
[17] M. Aaboud *et al.* (ATLAS Collaboration), J. High Energy Phys. 10 (2018) 047.
[18] A. J. Buras and J. Girrbach, J. High Energy Phys. 12 (2013) 009.
[19] R. Gauld, F. Goertz, and U. Haisch, J. High Energy Phys. 01 (2014) 069.
[20] W. Altmannshofer, J. Davighi, and M. Nardecchia, Phys. Rev. D **101**, 015004 (2020).
[21] S. Lebbal, N. Mebarki, and J. Mimouni, arXiv:2003.03230.
[22] B. Capdevila, A. Crivellin, C. A. Manzari, and M. Montull, arXiv:2005.13542.
[23] M. Bauer and M. Neubert, Phys. Rev. Lett. **116**, 141802 (2016).
[24] A. Angelescu, D. Bečirević, D. Faroughy, and O. Sumensari, J. High Energy Phys. 10 (2018) 183.
[25] A. Angelescu, arXiv:1905.06044.
[26] S. Balaji and M. A. Schmidt, Phys. Rev. D **101**, 015026 (2020).
[27] A. Crivellin, D. Müller, and F. Saturnino, J. High Energy Phys. 06 (2020) 020.
[28] S. Saad and A. Thapa, Phys. Rev. D **102**, 015014 (2020).
[29] J. Fuentes-Martín and P. Stangl, arXiv:2004.11376.

[30] B. Capdevila, A. Crivellin, S. Descotes-Genon, J. Matias, and J. Virto, J. High Energy Phys. 01 (2018) 093.
[31] Y. Li and C. D. Lü, Sci. Bull. **63**, 267 (2018).
[32] S. Bifani, S. Descotes-Genon, A. R. Vidal, and M. H. Schune, J. Phys. G **46**, 023001 (2019).
[33] B. Gripaios, M. Nardecchia, and S. Renner, J. High Energy Phys. 06 (2016) 083.
[34] P. Arnan, L. Hofer, F. Mescia, and A. Crivellin, J. High Energy Phys. 04 (2017) 043.
[35] P. Arnan, A. Crivellin, M. Fedele, and F. Mescia, J. High Energy Phys. 06 (2019) 118.
[36] Q. Y. Hu and L. L. Huang, Phys. Rev. D **101**, 035030 (2020).
[37] Q. Y. Hu, Y. D. Yang, and M. D. Zheng, Eur. Phys. J. C **80**, 365 (2020).
[38] L. Alasfar, A. Azatov, J. de Blas, A. Paul, and M. Valli, arXiv:2007.04400.
[39] M. Tanabashi *et al.* (Particle Data Group), Phys. Rev. D **98**, 030001 (2018).
[40] T. Gorringe and D. Hertzog, Prog. Part. Nucl. Phys. **84**, 73 (2015).
[41] T. Blum, P. A. Boyle, V. Gülpers, T. Izubuchi, L. Jin, C. Jung, A. Jüttner, C. Lehner, A. Portelli, and J. T. Tsang (RBC and UKQCD Collaborations), Phys. Rev. Lett. **121**, 022003 (2018).
[42] G. Bennett *et al.* (Muon g-2 Collaboration), Phys. Rev. D **73**, 072003 (2006).
[43] J-PARC (G-2/EDM Collaboration), AIP Conf. Proc. **1467**, 45 (2012).
[44] J. Grange *et al.* (Muon g-2 Collaboration), arXiv:1501.06858.
[45] L. Bergstrom, Ann. Phys. (Berlin) **524**, 479 (2012).
[46] P. Ade *et al.* (Planck Collaboration), Astron. Astrophys. **594**, A13 (2016).
[47] A. Vicente, Adv. High Energy Phys. **2018**, 3905848 (2018).
[48] D. A. Sierra, F. Staub, and A. Vicente, Phys. Rev. D **92**, 015001 (2015).
[49] G. Bélanger, C. Delaunay, and S. Westhoff, Phys. Rev. D **92**, 055021 (2015).
[50] W. Altmannshofer, S. Gori, S. Profumo, and F. S. Queiroz, J. High Energy Phys. 12 (2016) 106.
[51] A. Celis, W. Z. Feng, and M. Vollmann, Phys. Rev. D **95**, 035018 (2017).
[52] J. M. Cline, J. M. Cornell, D. London, and R. Watanabe, Phys. Rev. D **95**, 095015 (2017).
[53] J. Ellis, M. Fairbairn, and P. Tunney, Eur. Phys. J. C **78**, 238 (2018).
[54] S. Baek, Phys. Lett. B **781**, 376 (2018).
[55] K. Fuyuto, H. L. Li, and J. H. Yu, Phys. Rev. D **97**, 115003 (2018).
[56] P. Cox, C. Han, and T. T. Yanagida, J. Cosmol. Astropart. Phys. 01 (2018) 029.
[57] A. Falkowski, S. F. King, E. Perdomo, and M. Pierre, J. High Energy Phys. 08 (2018) 061.
[58] L. Darmé, K. Kowalska, L. Roszkowski, and E. M. Sessolo, J. High Energy Phys. 10 (2018) 052.
[59] S. Singirala, S. Sahoo, and R. Mohanta, Phys. Rev. D **99**, 035042 (2019).
[60] S. Baek and C. Yu, J. High Energy Phys. 11 (2018) 054.
[61] A. Kamada, M. Yamada, and T. T. Yanagida, J. High Energy Phys. 03 (2019) 021.
[62] D. Guadagnoli, M. Reboud, and P. Stangl, arXiv:2005.10117.
[63] I. de Medeiros Varzielas and O. Fischer, J. High Energy Phys. 01 (2016) 160.
[64] J. M. Cline, Phys. Rev. D **97**, 015013 (2018).
[65] C. Hati, G. Kumar, J. Orloff, and A. M. Teixeira, J. High Energy Phys. 11 (2018) 011.
[66] S. M. Choi, Y. J. Kang, H. M. Lee, and T. G. Ro, J. High Energy Phys. 10 (2018) 104.
[67] A. Datta, J. L. Feng, S. Kamali, and J. Kumar, Phys. Rev. D **101**, 035010 (2020).
[68] B. Bhattacharya, D. London, J. M. Cline, A. Datta, and G. Dupuis, Phys. Rev. D **92**, 115012 (2015).
[69] J. Kawamura, S. Okawa, and Y. Omura, Phys. Rev. D **96**, 075041 (2017).
[70] J. M. Cline and J. M. Cornell, Phys. Lett. B **782**, 232 (2018).
[71] D. Cerdeño, A. Cheek, P. Martín-Ramiro, and J. Moreno, Eur. Phys. J. C **79**, 517 (2019).
[72] B. Barman, D. Borah, L. Mukherjee, and S. Nandi, Phys. Rev. D **100**, 115010 (2019).
[73] L. Darmé, M. Fedele, K. Kowalska, and E. M. Sessolo, J. High Energy Phys. 08 (2020) 148.
[74] E. Ma, Phys. Rev. D **73**, 077301 (2006).
[75] E. Ma and D. Suematsu, Mod. Phys. Lett. A **24**, 583 (2009).
[76] E. Aprile *et al.* (XENON Collaboration), Phys. Rev. Lett. **121**, 111302 (2018).
[77] M. E. Peskin and T. Takeuchi, Phys. Rev. Lett. **65**, 964 (1990).
[78] M. E. Peskin and T. Takeuchi, Phys. Rev. D **46**, 381 (1992).
[79] W. Altmannshofer, P. Ball, A. Bharucha, A. J. Buras, D. M. Straub, and M. Wick, J. High Energy Phys. 01 (2009) 019.
[80] D. Becirevic, N. Kosnik, F. Mescia, and E. Schneider, Phys. Rev. D **86**, 034034 (2012).
[81] S. Descotes-Genon, L. Hofer, J. Matias, and J. Virto, J. High Energy Phys. 06 (2016) 092.
[82] T. Hurth, F. Mahmoudi, and S. Neshatpour, Nucl. Phys. **B909**, 737 (2016).
[83] W. Altmannshofer, P. Stangl, and D. M. Straub, Phys. Rev. D **96**, 055008 (2017).
[84] G. D'Amico, M. Nardecchia, P. Panci, F. Sannino, A. Strumia, R. Torre, and A. Urbano, J. High Energy Phys. 09 (2017) 010.
[85] G. Hiller and I. Nisandzic, Phys. Rev. D **96**, 035003 (2017).
[86] L. S. Geng, B. Grinstein, S. Jäger, J. M. Camalich, X. L. Ren, and R. X. Shi, Phys. Rev. D **96**, 093006 (2017).
[87] M. Ciuchini, A. M. Coutinho, M. Fedele, E. Franco, A. Paul, L. Silvestrini, and M. Valli, Eur. Phys. J. C **77**, 688 (2017).
[88] A. K. Alok, B. Bhattacharya, A. Datta, D. Kumar, J. Kumar, and D. London, Phys. Rev. D **96**, 095009 (2017).
[89] T. Hurth, F. Mahmoudi, D. M. Santos, and S. Neshatpour, Phys. Rev. D **96**, 095034 (2017).

[90] M. Algueró, B. Capdevila, A. Crivellin, S. Descotes-Genon, P. Masjuan, J. Matias, M. N. Brunet, and J. Virto, Eur. Phys. J. C **79**, 714 (2019); **80**, 511(A) (2020).
[91] S. Bhattacharya, A. Biswas, S. Nandi, and S. K. Patra, Phys. Rev. D **101**, 055025 (2020).
[92] R. Coy, M. Frigerio, F. Mescia, and O. Sumensari, Eur. Phys. J. C **80**, 52 (2020).
[93] A. Vicente, *Proc. Sci.*, Beauty2019 (2020) 029 [arXiv:2001.04788].
[94] A. Biswas, S. Nandi, I. Ray, and S. K. Patra, arXiv:2004.14687.
[95] J. Bhom, M. Chrzaszcz, F. Mahmoudi, M. Prim, P. Scott, and M. White, arXiv:2006.03489.
[96] A. Datta, J. Kumar, and D. London, Phys. Lett. B **797**, 134858 (2019).
[97] C. Bobeth, M. Gorbahn, T. Hermann, M. Misiak, E. Stamou, and M. Steinhauser, Phys. Rev. Lett. **112**, 101801 (2014).
[98] R. Aaij *et al.* (LHCb Collaboration), Phys. Rev. Lett. **118**, 191801 (2017).
[99] A. Bazavov *et al.* (Fermilab Lattice and MILC Collaborations), Phys. Rev. D **93**, 113016 (2016).
[100] N. Carrasco *et al.* (ETM Collaboration), J. High Energy Phys. 03 (2014) 016.
[101] D. King, A. Lenz, and T. Rauh, J. High Energy Phys. 05 (2019) 034.
[102] S. Aoki *et al.* (Flavour Lattice Averaging Group), Eur. Phys. J. C **80**, 113 (2020).
[103] F. Gabbiani, E. Gabrielli, A. Masiero, and L. Silvestrini, Nucl. Phys. **B477**, 321 (1996).
[104] L. Di Luzio, M. Kirk, and A. Lenz, arXiv:1811.12884.
[105] L. Di Luzio, M. Kirk, and A. Lenz, Phys. Rev. D **97**, 095035 (2018).
[106] Y. Amhis *et al.* (HFLAV Collaboration), Eur. Phys. J. C **77**, 895 (2017).
[107] M. Misiak *et al.*, Phys. Rev. Lett. **114**, 221801 (2015).
[108] M. Misiak, A. Rehman, and M. Steinhauser, Phys. Lett. B **770**, 431 (2017).
[109] P. Gondolo and G. Gelmini, Nucl. Phys. **B360**, 145 (1991).
[110] G. Belanger, F. Boudjema, A. Pukhov, and A. Semenov, Comput. Phys. Commun. **176**, 367 (2007).
[111] G. Bélanger, F. Boudjema, A. Pukhov, and A. Semenov, Comput. Phys. Commun. **192**, 322 (2015).
[112] J. M. Cline, K. Kainulainen, P. Scott, and C. Weniger, Phys. Rev. D **88**, 055025 (2013).
[113] J. Alarcon, J. M. Camalich, and J. Oller, Phys. Rev. D **85**, 051503 (2012).
[114] X. L. Ren, X. Z. Ling, and L. S. Geng, Phys. Lett. B **783**, 7 (2018).
[115] P. Achard *et al.* (L3 Collaboration), Phys. Lett. B **517**, 75 (2001).
[116] J. L. Feng, Annu. Rev. Astron. Astrophys. **48**, 495 (2010).
[117] ATLAS Collaboration, Search for electroweak production of supersymmetric particles in the two and three lepton final state at $\sqrt{s} = 13$ TeV with the ATLAS detector, Report No. ATLAS-CONF-2017-039.
[118] M. Aaboud *et al.* (ATLAS Collaboration), Eur. Phys. J. C **78**, 18 (2018).
[119] https://ncn.gov.pl/finansowanie-nauki/konkursy/typy/4?language=en.